

## First Results from AMANDA using the TWR System

ANDREA SILVESTRI<sup>†</sup> for the IceCube Collaboration\*

*Department of Physics and Astronomy, University of California  
Irvine, CA 92697, U.S.A.*

<sup>†</sup>*E-mail: silvestr@uci.edu*

The Antarctic Muon And Neutrino Detector Array (AMANDA) has been taking data since 2000 and its data acquisition system was upgraded in January 2003 to read out the complete digitized waveforms from the buried Photomultipliers (PMTs) using Transient Waveform Recorders (TWR). This system currently runs in parallel with the standard AMANDA data acquisition system. Once AMANDA is incorporated into the 1 km<sup>3</sup> detector IceCube, only the TWR system will be kept. We report results from a first atmospheric neutrino analysis on data collected in 2003 with TWR. Good agreement in event rate and angular distribution verify the performance of the TWR system. A search of the northern hemisphere for localized event clusters shows no statistically significant excess, thus a flux limit is calculated, which is in full agreement with previous results based on the standard AMANDA data acquisition system. We also update the status of a search for diffusely distributed neutrinos with ultra high energy (UHE) using data collected by the TWR system.

*Keywords:* Neutrino Detector, Neutrino Astronomy, Point Sources, Diffuse Sources, Ultra High Energy Neutrinos, AMANDA, TWR, IceCube

### Introduction

Neutrinos are the only high energy particles able to propagate undeflected and unattenuated from the furthest reaches of the Universe. Extragalactic UHE  $\gamma$ -ray astronomy falters for energies greater than a few tens of TeV due to interactions with infrared and Cosmic Microwave Background photons. The information carried by the neutrino messengers from distant, unexplored regions of the universe may help to unravel longstanding mysteries associated with the origin of the highest energy cosmic rays. Several models<sup>1, 2, 3, 4, 5, 6</sup> predict high energy charged particle and neutrino emission; the diffuse  $\nu$ -flux predictions by these models are constrained by

---

\*<http://www.icecube.wisc.edu>

the observed cosmic ray fluxes<sup>7</sup>. AMANDA<sup>8</sup>, the first neutrino telescope constructed in transparent ice, is deployed between 1500 m and 2000 m beneath the surface at the geographic South Pole. It is designed to search for neutrinos that originate in the most violent phenomena in the observable universe. Galactic objects like Supernova Remnants (SNR) and extragalactic objects such as Active Galactic Nuclei (AGN) are expected to be the powerful engines accelerating protons and nuclei to the highest energies, which eventually interact to generate neutrinos. We have searched for point sources in the northern sky and for a diffuse flux of UHE ( $E_\nu > 10^{15}$  eV) neutrinos of cosmic origin. We have performed the analysis using data collected in 2003 with a new data acquisition system based on Transient Waveform Recorders (TWR-DAQ), which we compared to data collected by the standard AMANDA readout system ( $\mu$ -DAQ).



Fig. 1. The upgraded AMANDA data acquisition electronics with Transient Waveform Recorders, here displayed in a system of 2 racks with 72 TWR modules.

### 1. The TWR System

The data acquisition electronics of the AMANDA-II detector (Fig. 1) was upgraded in 2003 to read out the complete digitized waveform of the photomultiplier tubes (PMTs) using Transient Waveform Recorders (TWR)<sup>9</sup>. The transition was made to run the  $\mu$ -DAQ<sup>10</sup> and TWR-DAQ in parallel to verify that the performance of the latter is as good or better. To compare

the two systems, the data from 2003 has been analyzed with data sets from both readout systems. The performance of the TWR-DAQ is verified by comparing the results for the absolute rate of atmospheric neutrinos and the  $\cos(\theta)$  distribution with the results from the standard  $\mu$ -DAQ<sup>11</sup>. Extending the analysis tools to include TWR data required several new developments: (1) The TWR-DAQ measures the integrated charge  $Q$  from the full waveform of the PMT pulses, in contrast, the  $\mu$ -DAQ only measures the maximum amplitude of the PMT pulse in a  $2 \mu\text{s}$  window. (2) Various time offsets were taken into account for the TWR-system, none of which impacted the  $\mu$ -DAQ. A time resolution of few nanoseconds was extracted. (3) The size of the TWR-DAQ data set (20TB for 2003) by far exceeds that of the  $\mu$ -DAQ ( $\sim 1\text{TB}$ ), requiring an improved data handling tools.

## 2. Analysis

The data information of the two systems has been merged according to GPS time and the fraction of overlapping PMTs participating in the event in both systems. For the point source analysis we restricted the capabilities of the TWR-DAQ system to mimic the features of the  $\mu$ -DAQ system as closely as possible. The timing and amplitude information extracted from waveforms has been used as input parameters to perform PMT-pulse cleaning, TOT (Time-Over-Threshold) and crosstalk<sup>a</sup> cleaning. A Gaussian fit of the

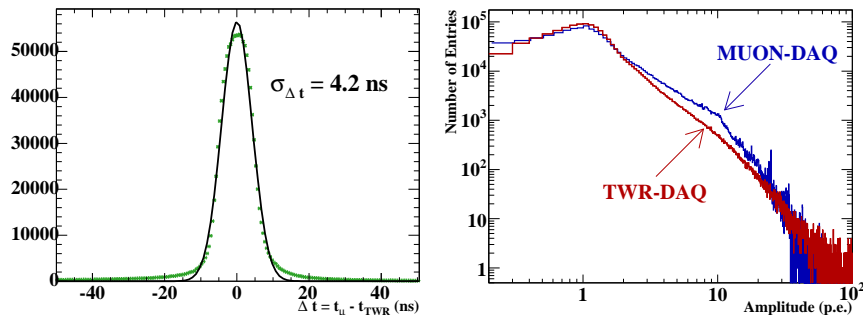


Fig. 2. (Left) Time difference between the PMT pulses recorded by the two acquisition systems  $\Delta t = t_\mu - t_{TWR}$ . (Right) Calibrated amplitude normalized to 1 photo-electron (p.e.) value for  $\mu$ -DAQ and TWR-DAQ data. See text for details.

<sup>a</sup> Any phenomenon by which a signal transmitted on one channel of a transmission system creates an undesired effect in another channel.

distribution for  $\Delta t = t_\mu - t_{TWR}$  yields  $\sigma_{\Delta t} = 4.2$  ns (Fig. 2 (left)), which is dominated by the systematic error of the time jitter between independent flash ADC clocks of the TWR system. The TWR-DAQ timing calculations are relative to the values measured by the  $\mu$ -DAQ. The timing of the TWR-DAQ system includes two sources of jitter, the digitization window of 10 ns and the time fluctuation of the flash ADC clocks within the same 10 ns interval. This accounts for the  $\sigma_{\Delta t} \sim 4$  ns<sup>b</sup>. Amplitudes are also calibrated by extracting the number of photo-electrons (Npe) detected from the peak ADC of the  $\mu$ -DAQ and charge  $Q$  of the TWR system and normalized to 1-pe amplitude. By integrating the charge from pulses in the waveform, the dynamic range of the TWR-DAQ extends to Npe of  $\sim 100$ , a factor of three higher than the  $\mu$ -DAQ. Fig. 2 (right) shows the reconstructed amplitude of the TWR-DAQ compared to the  $\mu$ -DAQ, which indicates a stable power law distribution extending up to 100 Npe, while the  $\mu$ -DAQ system shows a “knee” around 10 Npe. The knee is due to the amplitude saturation of channels read out by optical fibers, which comprise  $\sim 40\%$  of the AMANDA channels.<sup>c</sup> After cleaning, the muon track is reconstructed from the pulse times of the PMTs. Details on the reconstruction techniques can be found in<sup>12</sup>. Table 1

Table 1. Passing rates for increasing level of data selection criteria for the TWR-DAQ and  $\mu$ -DAQ data analysis.

Selection	TWR-DAQ	$\mu$ -DAQ
Level-0 (Raw)	$1.86 \times 10^9$	$1.86 \times 10^9$
Level-1	$1.25 \times 10^8$	$1.25 \times 10^8$
Level-2	$2.56 \times 10^6$	$1.99 \times 10^6$
Level-3 (Final)	1112	1026

summarizes the passing rates from the raw data level to the final sample of atmospheric neutrinos. The event selection criteria used in this analysis follows the method described in<sup>13</sup>. Fig. 3 shows that the angular mismatch for the final neutrino sample  $\sigma_{\Delta\theta}$  is  $0.5^\circ$  where  $\Delta\theta = \theta_\mu - \theta_{TWR}$ . This value is expected from studies of the precision of the global minimizer in the reconstruction program, by reconstructing the same event sample twice with a 32-iteration algorithm. The azimuth angular mismatch  $\sigma_{\Delta\phi}$  is  $0.7^\circ$ , which

<sup>b</sup>For year 2005 the phases of the TWR modules were synchronized to avoid the time jitter between independent flash ADC clocks.

<sup>c</sup>High voltage values were lowered in January 2005 to increase linear dynamic range of optical channels.

is consistent with a  $\sigma$  of  $0.5^\circ$  for the  $\Delta\phi \times \sin(\theta)$  distribution to account for the zenith dependence on the azimuth angle.

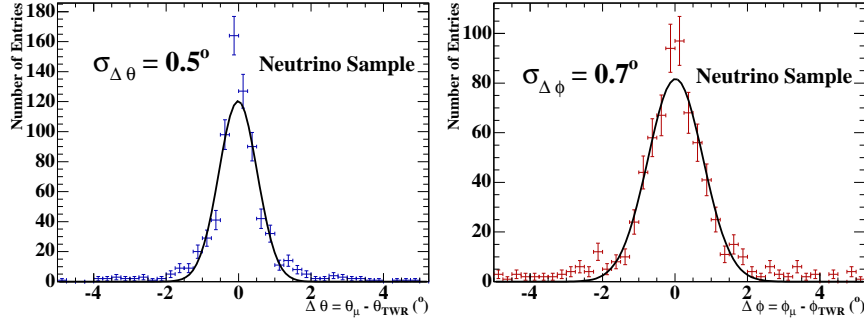


Fig. 3. (Left) The zenith  $\Delta\theta = \theta_\mu - \theta_{TWR}$  difference distribution between the  $\mu$ -DAQ and the TWR-DAQ systems, (right) the azimuthal  $\Delta\phi = \phi_\mu - \phi_{TWR}$  difference distribution.

### 3. Search for Point Sources of Neutrinos

From the analysis based on TWR-DAQ data, 1112 neutrinos are observed compared to 1026 neutrinos from the  $\mu$ -DAQ data analysis. The small differences in the event rate are compatible with the small differences in analysis procedures described in Section 2. Fig. 4 shows the  $\cos(\theta)$  distribution of the

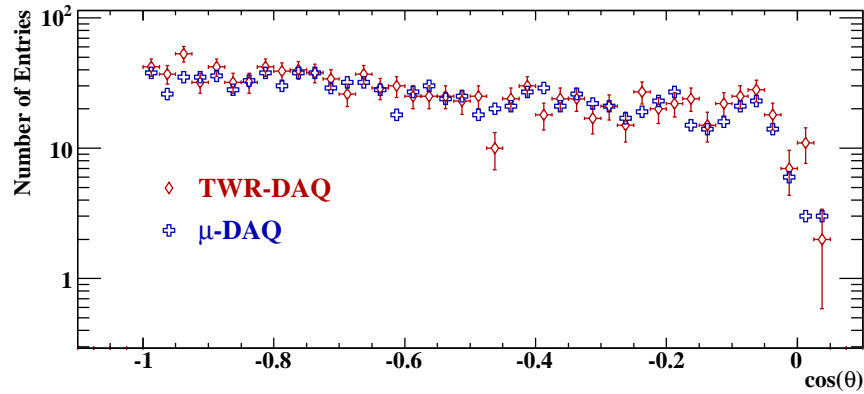


Fig. 4. Distribution of  $\cos(\theta)$  after final selection representing the atmospheric neutrino sample observed from the TWR-DAQ and the  $\mu$ -DAQ analyses.

6

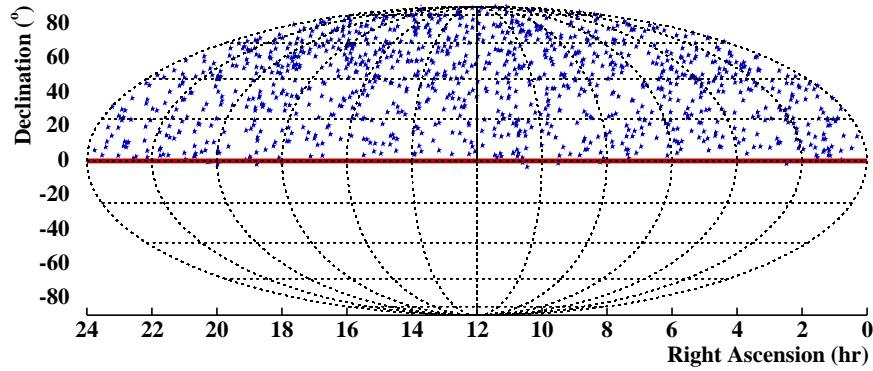


Fig. 5. Sky plot displayed in equatorial coordinates, Right Ascension (RA) and Declination (DEC), of the final sample of 1112 atmospheric neutrinos observed from the TWR-DAQ analysis.

atmospheric neutrino sample extracted from the TWR-DAQ and  $\mu$ -DAQ data analysis. Satisfactory agreement can be seen for the  $\cos(\theta)$  distribution of the atmospheric neutrinos samples obtained by the different analyses. Fig. 5 displays the sky map plotted in equatorial coordinates of the 1112 atmospheric neutrino candidates observed from the TWR-DAQ analysis. All events are distributed in the norther hemisphere with very few events reconstructed at the horizon. In order to distinguish if the observed events follow a random distribution as expected by atmospheric neutrinos, or are an indication of localized event cluster as expected by a source of neutrinos

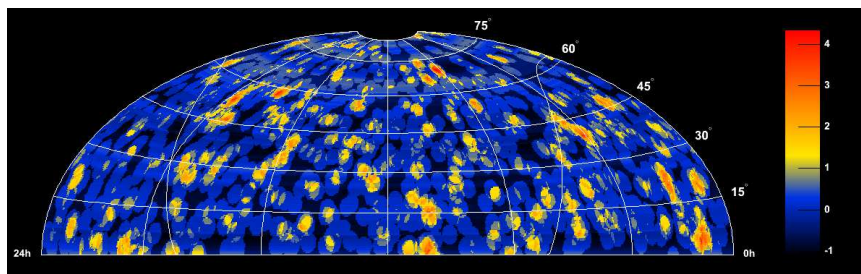


Fig. 6. Sky map plotted in coordinates of right ascension and declination of the 1112 atmospheric neutrino candidates from the TWR-DAQ analysis. The scale on the right reflects excess or deficit in terms of the positive or negative deviation with respect to the mean background events.

of extraterrestrial origin, an analysis is required to estimate the statistical significance of the observed events. A full search of the northern sky was performed to look for any localized event cluster. The full scan is extended to  $85^\circ$  in declination, since the limited statistics in the polar bin prevents an accurate estimate of the background. Fig. 6 shows the sky map of the calculated significance for all observed 1112 events in terms of the a positive or negative deviation with respect to the mean background events. All observed regions with the highest significance are compatible with the background hypothesis. The highest significance observed shows a positive deviation of  $4.3 \sigma$ , which corresponds to a probability of 23% for a search performed on events with randomized right ascension.

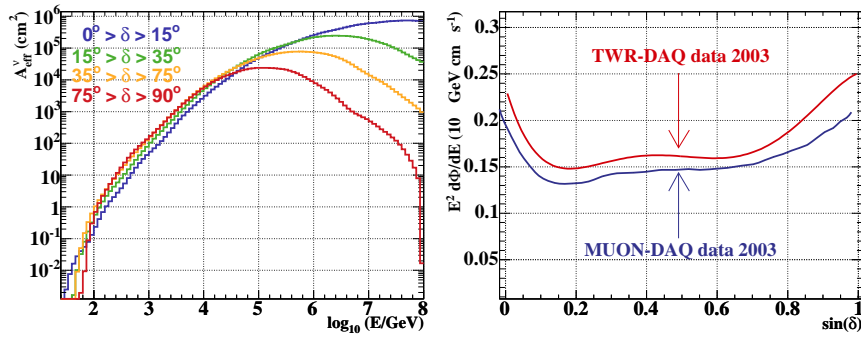


Fig. 7. (Left) Muon neutrino effective area as a function of  $E_{\nu_\mu}$  for point source searches displayed for different declinations  $\delta$ . (Right) Average upper limit as a function of  $\sin(\delta)$  on  $\nu_\mu$  for a  $E^{-2}$  neutrino flux spectrum from the TWR-DAQ and the  $\mu$ -DAQ analyses.

Numerous studies have been performed to implement the best possible description of the TWR system in the Monte Carlo simulation. In particular, a correct description of the waveform hardware response is now available and proper TDC time windows as well as amplitude calculations have been now implemented. Therefore a calculation of the neutrino effective area for point source search using TWR data is now feasible. Fig. 7 (left) shows the effective muon neutrino area as a function of  $E_{\nu_\mu}$  computed at the final selection of this analysis for four separated ranges of the declination. The  $A_{eff}^{\nu}$  extends over six order of magnitudes as  $\nu$ -energy increases, while  $A_{eff}^{\nu}$  decreases as declination increases due to the neutrino absorption in the Earth. The average upper limit on  $\nu_\mu$  as a function of declination is shown in the right panel of Fig. 7. The average neutrino flux upper limit is determined from the ratio of the average Feldman and Cousins<sup>14</sup> upper

limit  $\langle \mu^{90} \rangle$  computed according to the expected mean background and observed events, and the number of the expected signal events for a neutrino flux  $E_\nu^2 d\Phi_\nu/dE_\nu = \text{GeV s}^{-1}\text{cm}^{-2}$  from a point source at declination  $\delta$ . Together with the average upper limit extracted from the TWR-DAQ data, the limit from the  $\mu$ -DAQ data of year 2003<sup>13</sup> is also represented for comparison. These results are comparable, however the TWR-DAQ limit is  $\sim 10\%$  worse than the  $\mu$ -DAQ limit, because conservative event selection criteria have been applied that do not use the full waveform information in an optimal way. The preliminary average upper limit from the TWR-DAQ analysis on the muon neutrino flux with spectrum  $d\Phi_\nu/dE_\nu \propto E_\nu^{-2}$  is  $E_\nu^2 d\Phi_\nu/dE_\nu \leq 1.8 \times 10^{-7} \text{ GeV s}^{-1}\text{cm}^{-2}$  at 90% confidence level, in the energy range  $1.26 \text{ TeV} < E_\nu < 1.6 \text{ PeV}$ . This upper limit does not include systematic uncertainties. AMANDA has submitted a publication on a 5-year search for point sources (2000-2004) based on the  $\mu$ -DAQ data<sup>13</sup>, which improves the limit by  $\sim 67\%$  compared to the results from this analysis.

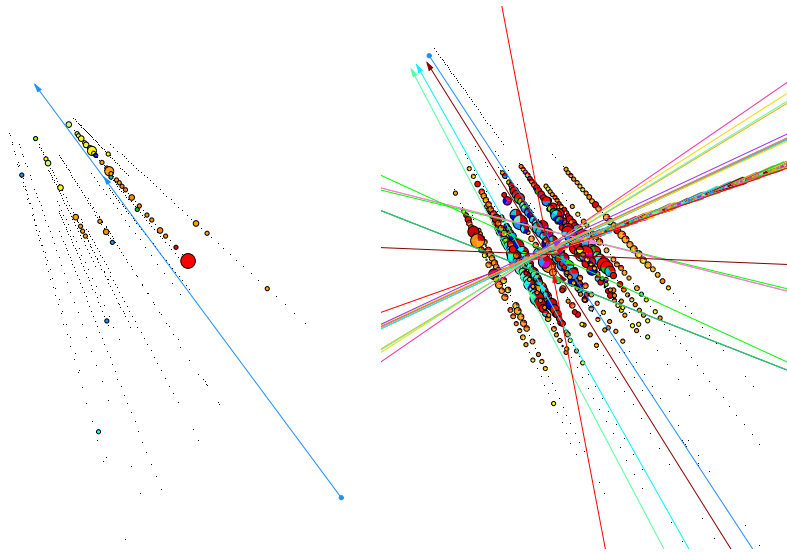


Fig. 8. (Left) one of the 1112 atmospheric neutrino event detected in the experimental array. (Right) a high-energy MC simulated event. The size of the circles represent energy deposited in the detector, the colors represent the time profile of photons propagating in the ice which have scattered to the PMTs.



#### 4. Search for UHE Neutrinos

The search for UHE neutrinos differs from the point source mainly in two aspects. First, the search for point sources is restricted to upward going events of energy within the TeV scale, the UHE analysis extends the search beyond PeV energies. Second, while point sources are localized in a small region of the sky, UHE diffuse neutrinos are expected to come from the entire visible sky ( $2\pi$  sr), with a higher probability to originate from the horizon. Fig. 8 shows one of the 1112 upward going neutrino events and an almost horizontal UHE simulated neutrino event with energy  $E \sim 3 \times 10^{15}$  eV. Simulated events with energy above one PeV deposit a substantial amount of light which is recorded by almost all PMTs. In order to better separate background events from signal events, we developed new variables which exploit the information of the full waveforms. The capability of improved

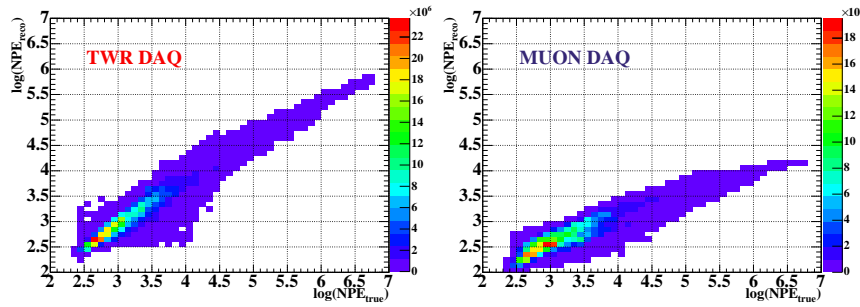


Fig. 9. Contour plots displaying the capability of correctly reconstructing the total number of photon-electron injected into the detector (left) for the TWR-DAQ and (right) for the  $\mu$ -DAQ system.

photo-electron reconstruction of the TWR-DAQ system can be seen in Fig. 9, which displays a contour plot in  $\log_{10}$ -scale of the sum of the reconstructed number of PE,  $NPE_{reco}$  versus the  $NPE_{true}$  generated by the signal MC simulation. While the  $\mu$ -DAQ system quickly saturates on the order of few thousands of PE's, the TWR-DAQ, by using the after-pulse information, can see the millions of PE's which are typical for UHE events triggered by single muons. Fig. 10 summarizes the results of several AMANDA searches for diffuse neutrinos at different energy ranges using  $\mu$ -DAQ data. The experimental limits assume a 1:1:1 ratio of neutrino flavors at the Earth due to oscillation. The dotted and dashed lines represent a sample of model predictions<sup>1, 2, 3, 4, 6</sup>, adjusted for oscillation if necessary. The horizontal

solid lines represent limits on the integrated neutrino flux from the diffuse analyses with AMANDA-B10<sup>15</sup>, with AMANDA-II<sup>16</sup>, from the cascade analysis<sup>17</sup>, and from the UHE analysis<sup>18, 19</sup>, with the NT200 neutrino telescope<sup>20</sup>, and at the highest energies from ANITA-lite<sup>21</sup> and RICE<sup>22</sup>. These are the most stringent flux limits at 90% C.L. for an  $E^{-2}$  spectrum to date. The AMANDA limits have been determined by analysing data collected with the  $\mu$ -DAQ system. However, as it has been shown above, by performing a new analysis approach with TWR-DAQ data, it is possible to develop new techniques and to improve the current experimental limits for the UHE neutrino search.

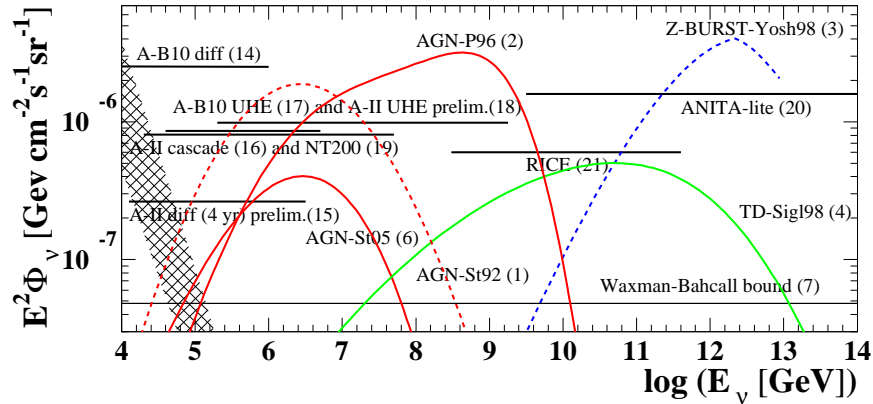


Fig. 10. Experimental limits on the integrated neutrino flux and detector sensitivity for a neutrino flux of  $E^{-2}$  spectrum. The curves represents predictions from theoretical models, the solid lines show current AMANDA (all-flavor limits), NT200, ANITA and RICE experimental limits.

## 5. Conclusion

The point source search provides the first detailed evaluation of the performance of the TWR-DAQ system. This analysis demonstrated that the TWR-DAQ produces similar event rates and angular distribution as the data collected by the standard  $\mu$ -DAQ system. No statistically significant excess has been observed after performing a full search of the northern hemisphere of the sky for localized event clusters, therefore a flux limit based on TWR-DAQ data is calculated. The AMANDA TWR readout is now being incorporated into the IceCube data acquisition system. By exploiting the information of

the full waveforms from the TWR-DAQ system, it is possible to develop new analysis techniques for an improved search for diffuse UHE neutrinos. Currently the AMANDA experiment has placed the most stringent neutrino flux limits to date, which can be further improved by analyses performed with TWR-DAQ data.

### Acknowledgments

The author acknowledges support from the U.S. National Science Foundation (NSF) Physics Division, the NSF-supported TeraGrid systems at the San Diego Supercomputer Center (SDSC) and the National Center for Supercomputing Applications (NCSA), the Phi Beta Kappa Alumni in Southern California for providing travel grants, the Astrophysics Associates, Inc., Italian Ministry of Education, European Physical Society, Ettore Majorana Foundation, and the Electron Tubes Ltd. for providing the full scholarship at Erice.

### References

1. F. Stecker et al., *Phys. Rev. Lett.* **66**, 2697 (1992).
2. R. J. Protheroe, *astro-ph/9607165* (1996).
3. S. Yoshida et al., *Phys. Rev. Lett.* **81**, 5505-5508 (1998).
4. G. Sigl, *Phys. Rev. D* **59**, 043504 (1999).
5. R. Engel et al., *Phys. Rev. D* **64**, 093010 (2001).
6. F. W. Stecker, *Phys. Rev. D* **72**, 107301 (2005).
7. E. Waxman and J. Bahcall, *Phys. Rev. D* **59**, 023002 (1999).
8. A. Silvestri et al., in *Neutrinos and Explosive Events in the Universe*, Springer, New-York, **209**, 275-285 (2005).
9. W. Wagner et al., in *28th ICRC*, **2**, 1365-1368 (2003).
10. R. Wischnewski et al., in *27th ICRC*, **2**, 1105-1108 (2001).
11. A. Silvestri et al., in *29th ICRC*, **5**, 431-434 (2005).
12. J. Ahrens et al., *Nucl. Instrum. Meth.* **A524**, 169 (2004).
13. A. Achterberg et al., *astro-ph/0611063* (2006).
14. G. J. Feldman and R. D. Cousins, *Phys. Rev. D* **57**, 3873 (1998).
15. J. Ahrens et al., *Phys. Rev. Lett.* **90**, 251101 (2003).
16. G. Hill et al., in Proc. of the XXII International Conference on Neutrino Physics and Astrophysics (2006).
17. M. Ackermann et al., *Astropart. Phys.* **22**, 127 (2005).
18. M. Ackermann et al., *Astropart. Phys.* **22**, 339 (2005).
19. L. Gerhardt et al., in Proc. of SUSY06 (2006).
20. V. Aynutdinov et al., *Astropart. Phys.* **25**, 140 (2006).
21. S. Barwick et al., *Phys. Rev. Lett.* **96**, 171101 (2006).
22. I. Kravchenko et al., *Phys. Rev. D* **73**, 082002 (2006).